

AFRL-VA-WP-TP-2003-308

**DEVELOPMENT & VALIDATION OF
AIRFOILS FOR GLOBAL RANGE
TRANSPORTS**

**Carl P. Tilmann
Lee B. Brandt
Justin W. Russell
Robyn Reuss Ramsay
Thomas Höhn**



AUGUST 2000

Approved for public release; distribution is unlimited.

This material is declared a work of the U.S. Government and is not subject to copyright protection in the United States.

**AIR VEHICLES DIRECTORATE
AIR FORCE RESEARCH LABORATORY
AIR FORCE MATERIEL COMMAND
WRIGHT-PATTERSON AIR FORCE BASE, OH 45433-7542**

20030516 051

REPORT DOCUMENTATION PAGE				Form Approved OMB No. 0704-0188	
The public reporting burden for this collection of information is estimated to average 1 hour per response, including the time for reviewing instructions, searching existing data sources, gathering and maintaining the data needed, and completing and reviewing the collection of information. Send comments regarding this burden estimate or any other aspect of this collection of information, including suggestions for reducing this burden, to Department of Defense, Washington Headquarters Services, Directorate for Information Operations and Reports (0704-0188), 1215 Jefferson Davis Highway, Suite 1204, Arlington, VA 22202-4302. Respondents should be aware that notwithstanding any other provision of law, no person shall be subject to any penalty for failing to comply with a collection of information if it does not display a currently valid OMB control number. PLEASE DO NOT RETURN YOUR FORM TO THE ABOVE ADDRESS.					
1. REPORT DATE (DD-MM-YY) August 2000		2. REPORT TYPE Conference Paper		3. DATES COVERED (From - To)	
4. TITLE AND SUBTITLE DEVELOPMENT & VALIDATION OF AIRFOILS FOR GLOBAL RANGE TRANSPORTS				5a. CONTRACT NUMBER In-house	
				5b. GRANT NUMBER	
				5c. PROGRAM ELEMENT NUMBER 61102F	
				5d. PROJECT NUMBER 2304	
6. AUTHOR(S) Carl P. Tilmann (AFRL/VAAA) Lee B. Brandt and Justin W. Russell (Lockheed Martin Aeronautics Company) Robyn Reuss Ramsay (The Ohio State University) Thomas Höhn (Federal Office of Military Technology & Procurement (BWB))				5e. TASK NUMBER N4	
				5f. WORK UNIT NUMBER 01	
7. PERFORMING ORGANIZATION NAME(S) AND ADDRESS(ES) <div style="display: flex; justify-content: space-between;"> <div style="width: 45%;"> Aerodynamic Configuration Branch (AFRL/VAAA) Aeronautical Sciences Division Air Vehicles Directorate Air Force Research Laboratory, Air Force Materiel Command Wright-Patterson Air Force Base, OH 45433-7542 </div> <div style="width: 45%;"> Lockheed Martin Aeronautics Company The Ohio State University Federal Office of Military Technology & Procurement (BWB) </div> </div>				8. PERFORMING ORGANIZATION REPORT NUMBER AFRL-VA-WP-TP-2003-308	
9. SPONSORING/MONITORING AGENCY NAME(S) AND ADDRESS(ES) Air Vehicles Directorate Air Force Research Laboratory Air Force Materiel Command Wright-Patterson Air Force Base, OH 45433-7542				10. SPONSORING/MONITORING AGENCY ACRONYM(S) AFRL/VAAA	
				11. SPONSORING/MONITORING AGENCY REPORT NUMBER(S) AFRL-VA-WP-TP-2003-308	
12. DISTRIBUTION/AVAILABILITY STATEMENT Approved for public release; distribution is unlimited.					
13. SUPPLEMENTARY NOTES Presented at the 18th AIAA Applied Aerodynamics Conference, 14-17 August 2000, Denver, CO. This material is declared a work of the U.S. Government and is not subject to copyright protection in the United States.					
14. ABSTRACT The developmental process for an airfoil designed to be used on long-range transonic transport aircraft with large regions of natural laminar flow is described. Components of the development process that are discussed include mission-driven needs criteria, airfoil design method, experimental airfoil validation, and a variety of numerical validation procedures. Numerical analyses include flowfield prediction, boundary layer stability analysis and transition prediction, and force and moment assessment. Assessments are made at several off-design conditions. The overall goal is to develop and demonstrate the computational tools and analytical methods required for the optimal design of unconventional airfoils and wings for global range cruise flight.					
15. SUBJECT TERMS					
16. SECURITY CLASSIFICATION OF:			17. LIMITATION OF ABSTRACT: SAR	18. NUMBER OF PAGES 20	19a. NAME OF RESPONSIBLE PERSON (Monitor) Carl P. Tilmann 19b. TELEPHONE NUMBER (Include Area Code) (937) 255-4077
a. REPORT Unclassified	b. ABSTRACT Unclassified	c. THIS PAGE Unclassified			

DEVELOPMENT & VALIDATION OF AIRFOILS FOR GLOBAL RANGE TRANSPORTS

Carl P. Tilmann*

Air Force Research Laboratory, Air Vehicles Directorate, Aeronautical Sciences Division
2130 8th Street, Wright Patterson AFB, Ohio 45433-7542

Lee B. Brandt† & Justin W. Russell‡

Lockheed Martin Aeronautics Company
86 South Cobb Drive, Marietta, Georgia 30063-0264

Robyn Reuss Ramsay§

The Ohio State University, Aeronautical and Astronautical Research Laboratory
2300 West Case Road, Columbus, Ohio 43235-2533

Thomas Höhn¶

Federal Office of Military Technology & Procurement (BWB), Aircraft and Aeronautical Equipment Division
P.O. Box 30 01 65, 56057, Koblenz, Germany

Abstract

The developmental process for an airfoil designed to be used on long-range transonic transport aircraft with large regions of natural laminar flow is described. Components of the development process that are discussed include mission-driven needs criteria, airfoil design method, experimental airfoil validation, and a variety of numerical validation procedures. Numerical analyses include flowfield prediction, boundary layer stability analysis and transition prediction, and force and moment assessment. Assessments are made at several off-design conditions. The overall goal is to develop and demonstrate the computational tools and analytical methods required for the optimal design of unconventional airfoils and wings for global range cruise flight.

Nomenclature

AR	= wing aspect ratio, $=b^2/S$
b	= wing span
c	= airfoil chord length
C_L	= airfoil section lift coefficient
C_D	= airfoil section drag coefficient
C_M	= airfoil section moment coefficient
$C_{M\alpha}$	= stability margin (per degree), $\partial C_M/\partial \alpha$
C_p	= pressure coefficient
L/D	= lift-to-drag ratio
M	= Mach number
N_{crit}	= critical amplification factor for e^N method
P	= static pressure
P_{t2}	= pitot pressure
P_t	= total plenum pressure
Re	= Reynolds number, $\rho_\infty u_\infty \ell / \mu_\infty$
Re_c	= chord Reynolds number, $\rho_\infty u_\infty c / \mu_\infty$
S	= wing planform area
TOGW	= takeoff gross weight
u,v,w	= mean Cartesian velocity components
α	= airfoil incidence angle (degrees)
μ	= viscosity
ρ	= density

* Research Aerospace Engineer, Senior Member AIAA.

† Engineer Staff

‡ Engineer Senior, Member AIAA.

§ Research Associate, Member AIAA.???

¶ Senior Aeronautical Engineer

1 Introduction

1.1 Background

This manuscript describes efforts conducted under an Air Force Research Laboratory program aimed at improving the aerodynamic performance of military transport aircraft. This program has supported the Air Force's *New World Vistas* (NWV) vision of *Global Mobility* by developing technology required to design wings for future 'global range' transports. Worldwide coverage could require aircraft that can fly up to 12,000 miles, deliver cargo, and return without refueling at the terminal point.¹ The *New World Vistas* report also states that "In general, it appears that wing research could pay off in significantly higher aircraft efficiencies." It is our belief that emerging technologies in active flow control, coupled with existing design methods may provide significant improvements in wing performance through drag reduction and lift enhancement. One of the primary objectives of AFRL's NWV program has been to develop and demonstrate the computational tools and analytical methods required to design active global range transport aircraft wings. This study has also been integrated into the Aerodynamic Configuration Branch's technical activities in flow control for drag reduction and separation management^{2,3}. The undertaking discussed in this paper comprises the first steps toward the ultimate goal of designing very high-performance powered airfoils.

1.2 Natural Laminar Flow Airfoils

Natural Laminar Flow (NLF) airfoils have been in use on high-performance sailplanes for decades, and have gained popularity in the general aviation and kit-plane markets more recently. This has involved been marked a steady progression in NLF airfoil development from low to moderate speed and Reynolds number operating environments. Furthermore, many tools are now available that allow the designer to custom-design airfoils^{4,5} and wings⁶ for specific applications. Due to these advances, many airfoils are now designed for the specific application for which they are intended, as opposed to choosing the most suitable airfoil available from a handbook or a catalog.

1.3 Summary of Present Work

Despite the advances in airfoil design methods, very few airfoils have been designed for NLF at transonic flight conditions. In addition, at high speed the design can become very sensitive to small changes in Mach number. In the present work, an airfoil family has been developed and tested for the specific application of a high-transonic speed long-range transport.

In this paper, we describe a process for developing an airfoil for long-range transonic transport aircraft having large regions of laminar flow. The overall goal is to develop and demonstrate the computational tools and analytical methods required to optimize transport aircraft airfoils and wings for global range cruise flight. The primary objectives of the study described in this paper were to:

- Establish mission requirements & airfoil design criteria.
- Design an airfoil specifically for an aircraft intended to meet the global range transport mission.
- Compare the performance of this family of airfoils to those existing in today's operational fleet at several operating conditions using common analysis methods.
- Assess current boundary layer stability methods for predicting transition on high-speed NLF airfoil designs.
- Perform highly instrumented high Reynolds number airfoil wind tunnel tests to validate design and analysis methods/models for NLF airfoil/wing development.

2 Aircraft Mission Requirements

To define the airfoil design conditions and constraints, it was first necessary to identify the various operating conditions of the aircraft on which the airfoil would be used. To accomplish this, it was first necessary to identify mission requirements based on educated forecasts about future operational requirements. Independent R&D studies by Lockheed Martin Aeronautics Company were used to establish mission requirements, wing design criteria. LMASC was also responsible for producing the airfoil design discussed in this paper. Previous Lockheed, NASA⁷, and Air Force mission studies were considered to

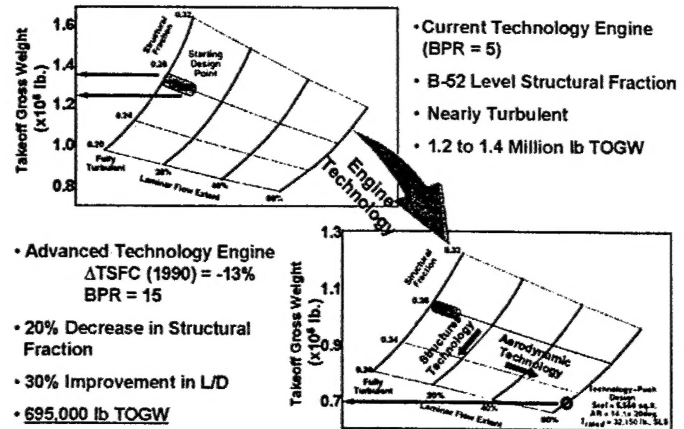


Figure 1: Global range transport propulsion, structures, and aerodynamic technology payoffs.

define the mission requirements. There have been several other system level studies that propose comparable requirements to meet the "global range" mission. These suggest similar aircraft characteristics when a conventional transonic monoplane configuration is the assumed. A distinction may be that we are requiring the aircraft to cruise at Mach numbers more typical of civil transports the slower flying military transports.

When assumed engine technology advances are established (reducing TSFC and increasing bypass ratio), the effects of structural and aerodynamic advances can be isolated. Figure 1 illustrates how structures technology (reducing structural weight fraction) and aerodynamic technology (in the form of laminar flow) both play a significant role in realizing potential takeoff gross weight (and cost) reductions. The mission requirements assumed for the present study are summarized in Table 1. The notional transport characteristics resulting from the assumed level technology infusion, including NLF, is described in Table 2 and illustrated in Figure 2.

3 Airfoil Design

A low-cost approach to airfoil design using the MSES^{5,8,9} computational airfoil development code is described here. The NLF airfoil development activity was worked in cooperation with the Lockheed Martin Aeronautics Company to insure that the airfoil geometry developed was compatible with military transport wing fabrication and control surface integration requirements.

3.1 Design Tool

MSES is a numerical airfoil design and analysis tool (developed at MIT) that includes capabilities to analyze, modify, and optimize 2-D single- and multi-element airfoils. For the present study, MSES version 2.8 was used. The method is valid for a wide range of Reynolds numbers and through transonic Mach numbers. Flows with transitional separation bubbles, shock waves, trailing edge and shock-induced separation can be simulated.

Table 1: Envisioned mission requirements & cruise flight conditions for a global range transport.

Parameter	Value
Range	12,000 NM
Cruise Mach Number	0.8
Cruise Altitude	34,500 ft
Re/l	$1.95 \times 10^6 \text{ ft}^{-1}$
Payload	150,000 lb

Table 2: Notional global range transport characteristics.

Parameter	Value
Takeoff Gross Weight	695,000 lb
Leading Edge Sweep	20°
Wing Area (S)	5560 ft^2
Span (b)	279 ft
Aspect Ratio	14.0
Chord Length	19.9 ft
Taper Ratio	0.2

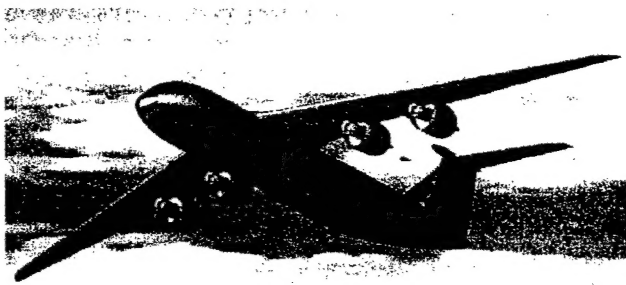


Figure 2: Conceptual long-range configuration.

Surface pressure and aerodynamic force predictions are accurate to just past stall. The laminar to turbulent location can be specified, or it can be predicted as part of the flow calculation.

MSES couples a streamline based Euler solver with a two-equation integral boundary layer method through the displacement thickness. The boundary layers and trailing wakes are simulated using a two-equation integral formulation with lagged-dissipation closure. The airfoil surfaces admit a solid-body boundary condition in the direct analysis mode, and a prescribed-pressure boundary condition in the inverse "design" mode. The overall system is solved using a full Newton method.

MSES uses a simplified version of the e^N method for transition prediction called the "envelope method". Instead of tracking the Tollmien-Schlichting (T-S) wave amplitudes for many individual frequencies (as in the e^N method), the envelope method determines for each

surface point the amplitude of whatever frequency happens to be most amplified at that point. This is a great simplification, but involves some approximations that have the greatest impact in flows where the shape parameter varies rapidly. The validity of the results of the envelope method can be easily checked in MSES by plotting amplitude of both the envelope as well as the amplifications for individual frequencies that *would have been* predicted by the e^N method¹⁰. Ideally, the envelope curve just touches the largest of all the individual frequency curves at each location. Any deviation from this ideal usually lies within the uncertainty in the specified critical amplification factor " N_{crit} ".

This tool was used here to design a natural laminar flow (NLF) transport aircraft airfoil that has a projected cruise L/D significantly higher than the turbulent airfoil designs currently used on long range military transport aircraft. The resulting family of airfoils has been nicknamed GRALF (Global Range Airfoil for Laminar Flow).

3.2 Airfoil Design Criteria & Constraints

Based on the assumed mission specifications for a global-range transport, the wing airfoil section needed to produce an on-design lift coefficient of 0.62 at a cruise Mach number of 0.75 and a unit Reynolds number of 1.83×10^6 per foot (Table 3). The objective in designing this airfoil is to generate a section that yields a long extent of natural laminar flow over both the upper and lower surfaces while limiting the shock strength (wave drag) on the upper surface. This will produce a significantly higher lift-to-drag ratio than typically seen on today's transport aircraft. The only constraint that was considered in this design was to limit the airfoil thickness to a *minimum* of 9% chord for structural reasons (though the resulting airfoil is actually 10.2% thick).

The design Reynolds number of the test airfoil (Table 4) was chosen to be 4.5×10^6 to match the typical operating range $Re/l = 9 \times 10^6 \text{ ft}^{-1}$ of the wind tunnel facility where validation testing was planned (Section 5.1.1). This value is of course an order of magnitude smaller than that expected in flight, but it was necessary to design at the testing Reynolds number to make the experiment meaningful. Designing for the higher Reynolds number would result in a very conservative airfoil, with an overly stable boundary layer in the tunnel.

A critical N -factor (N_{crit}) of 4 was assumed during the design process rather than the more typical value of about 9 that is usually used to predict transition in flight. While this is conservative, previous experience with two-dimensional testing at OSU has indicated that this value is a more characteristic value for the tunnel.

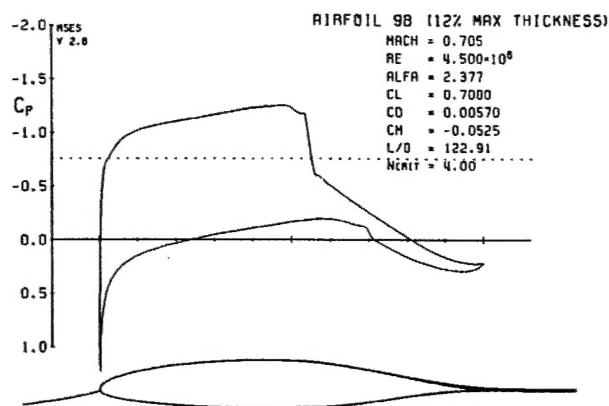


Figure 3: Airfoil 9B surface pressure distribution at its design condition.

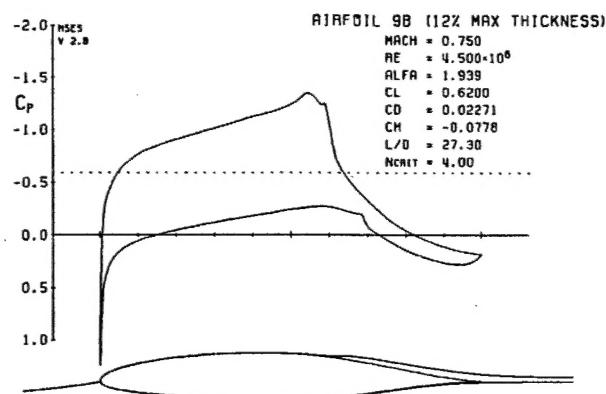


Figure 4: Airfoil 9B surface pressure distribution at GRT mission flight condition.

3.3 Airfoil Design Procedure

The starting point for designing this natural laminar flow airfoil was a section developed under Lockheed Martin Aeronautics Company IR&D for a different design condition (Figure 3). Note that this airfoil was also 4.5×10^6 to match the OSU wind tunnel operating conditions. The airfoil was chosen because the section was already known to produce an appreciable amount of laminar flow even at the conditions expected for the global-range transport (Figure 4). However, the upper surface contour results in a strong shock and hence much more wave drag at this higher Mach number. The definition of the design problem was thus to improve the section's laminar-flow characteristics for the given design operating conditions without violating the 9% thickness constraint or producing a large amount of wave drag.

To accomplish this, the inverse design capability of MSES was employed. This process involves producing an initial starting-point C_p distribution (as shown in Figure 4) which can be graphically manipulated (using the MEDP module) by the designer to produce a 'better' C_p distribution. The weakness of this methodology is that it

Table 3: Required airfoil section characteristics for notional global range transport of Table 2.

Parameter	Value
Mach Number	0.75
Lift Coefficient	0.62
Normal Chord Length	18.7 ft
Re/ℓ	$1.83 \times 10^6 \text{ ft}^{-1}$
Reynolds Number, Re_c	32.2×10^6
Minimum t/c	9%

Table 4: Design conditions for the GRALF test airfoil.

Parameter	Value
Mach Number	0.75
Lift Coefficient	0.62
Reynolds Number, Re_c	4.5×10^6
Minimum t/c	9%

requires some *a priori* knowledge of a "good" pressure distribution. However for the case at hand, where a good starting-point design is already known, this inverse method allows the designer to easily manipulate the section to produce the desired results. Based on experience, we know that to preserve laminar flow on the airfoil we must maintain a favorable pressure gradient along the chord of the airfoil section. The drawback of this is that a favorable pressure gradient causes the flow to accelerate over a long distance and can produce a strong shock wave on the upper surface of the section. Such a strong shock produces wave drag, which if not limited, can offset any gains achieved by maintaining laminar flow. The design of the C_p distribution is thus a tradeoff between maintaining laminar flow and the strength of the shock wave on the upper surface of the airfoil.

The starting-point airfoil design already produces a reasonable amount of laminar flow along the lower surface. Thus, most of the work involves manipulating the pressure distribution on the upper (suction) side of the airfoil. After the initial pressure distribution is manipulated, MSES is re-run in inverse-design mode. This produces a geometry that yields a minimum error between the actual and specified pressure distributions. This new geometry is then checked against the thickness constraint. If this constraint is not met, the geometry is simply scaled up to meet the minimum thickness requirement and a new C_p distribution is computed. Because this computed pressure distribution is likely to result in a different C_L than is desired, MSES is run again in standard solution mode to determine the angle-of-attack required to produce the design C_L for this new geometry. This process is repeated by importing this pressure distribution back into MEDP and manipulating it until a reasonable (as determined by the designer) pressure distribution is achieved.

The resulting 10.2% thick airfoil produces a shed-roof looking pressure distribution with the favorable pressure gradient needed to maintain laminar flow (Figure 5). The slope of the favorable pressure gradient on the forward part of the airfoil is limited to keep the shock strength in check on the aft section. The results predict that this yields a very high section L/D of 110, resulting from a predicted transition location of 56% chord on the upper surface and 69% chord on the lower surface. The locations and relative strengths of the primary shock and a secondary shock on the upper surface are evident the pressure field contours shown in Figure 6.

4 Analysis & Aerodynamic Predictions

The airfoil has been evaluated analytically using several methods varying complexity and sophistication. The MSES code, and varying levels of finite difference methods were used to evaluate the airfoil performance with varying levels of success depending on flow conditions and the desired information.

4.1 MSES Analysis

MSES, as described above, is a 2-D airfoil analysis and design tool that couples a streamline based Euler solver with a two-equation integral boundary layer method through the displacement thickness.

In Figure 7, the airfoil performance predicted by MSES is summarized in the form of lift, drag, and moment coefficients (C_L , C_D , C_M) and angle-of-attack (α). The influence of the assumed critical amplification factor (N_{crit}) for the e^N transition model primarily affects the range in C_L (or α) over which significant laminar flow can be maintained.

As would be anticipated, higher N_{crit} values lead to substantial laminar flow over a larger range in C_L . This is also evidenced by the growing extent of the 'laminar bucket' in the drag polar. Also shown is the case where transition is forced to occur (the boundary layer is "tripped") at 5% of the chord length on both the upper and lower surfaces. It should be mentioned that forcing the transition location in this way does not lead to an abrupt change in moment characteristics ($\partial C_M / \partial \alpha$), as is often the case for NLF airfoil designs.

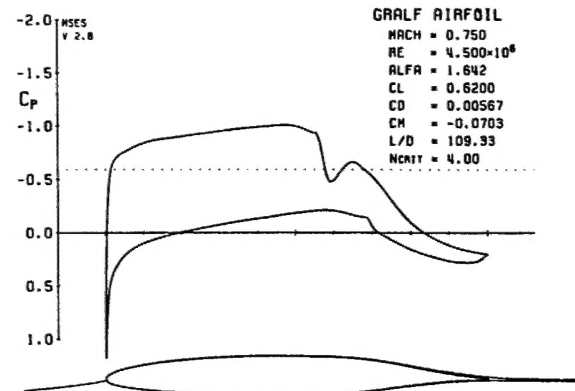


Figure 5: GRALF surface pressure distribution at design.

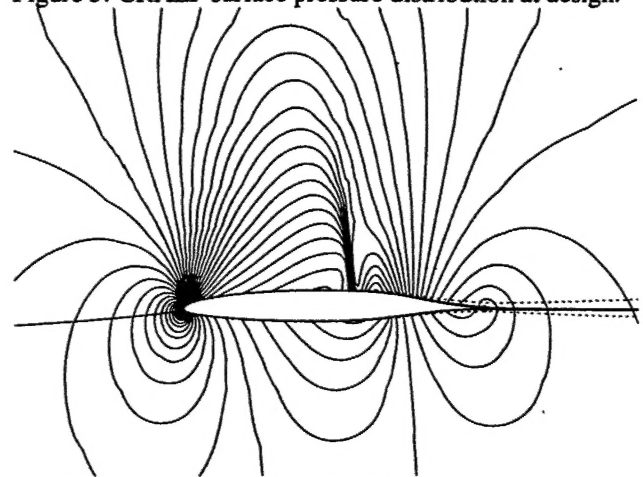


Figure 6: Pressure field of GRALF at design point.

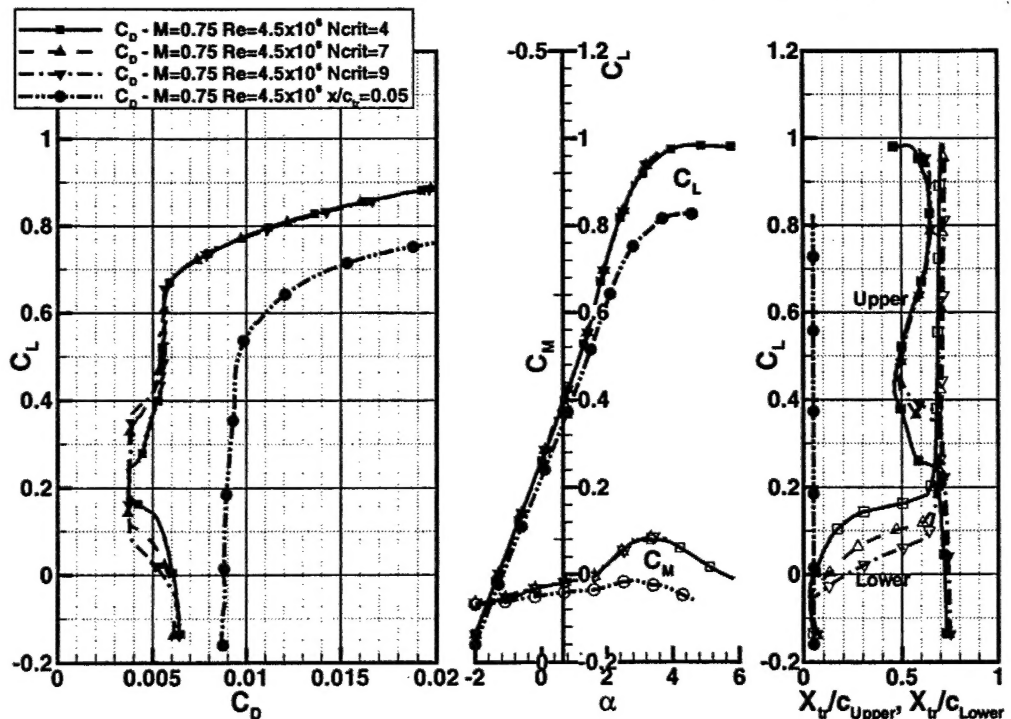


Figure 7: Airfoil performance predictions from MSES.

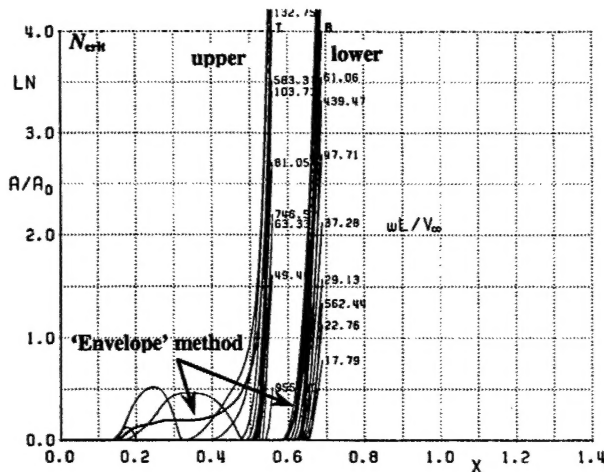


Figure 8: Disturbance growth at design condition.

Shown are predictions from envelope method, and by e^N method for several non-dimensional frequencies.

Above $C_L=0.25$, the transition location on the upper surface is predicted to move forward with increasing lift as is typical of NLF airfoils. For most NLF airfoils, this is due to the transition location moving forward as the lift increases. In this case however, for lift coefficients of 0.25 and above, the transition location was found to coincide with the appearance and movement of the upstream shock on the upper surface. For lift coefficients of 0.25 and above, the transition location closely follows the location of the shock on the upper surface. In the range $0.25 \leq C_L \leq 0.45$, the location of this shock appears to be somewhat dependent on N_{crit} . The low predicted disturbance amplifications shown in Figure 8 further illustrate that the amplifications are always well below the specified N_{crit} until the shock is encountered.

Figure 9 further illustrates the shock strengths and movement with increases in incidence and lift for $N_{crit}=4$. The aft shock develops at relatively low (nearly zero) lift condition, and increases in strength as lift is increased while maintaining nearly the same position. The forward shock begins to develop at a C_L of about 0.25, but remains weak and moves slightly forward at higher lift until $C_L=0.45$. As lift is further increased, this shock strengthens and moves rearward until it merges with the aft shock, forming a much stronger compression.

The sensitivity to varying Mach number (at a given incidence angle) is illustrated in Figure 10. Changes of only $\Delta M=0.02$ from the design point can significantly change the shock structure and location. At Mach numbers slightly above the design point, the forward shock quickly moves rearward. It merges with and strengthens the aft shock, which remains relatively stationary. Further effects of Mach number and Reynolds number will be discussed with the experimental results.

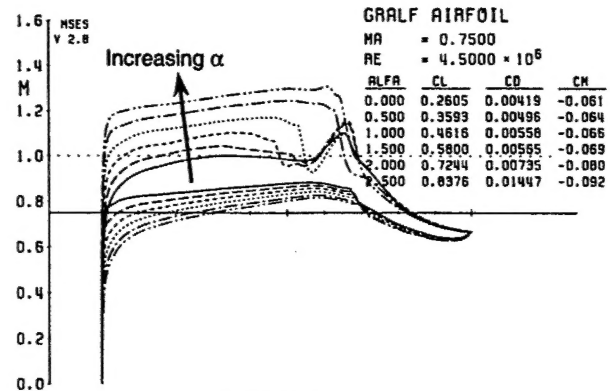


Figure 9: Effect of incidence (or lift) on boundary layer edge Mach number at design conditions.

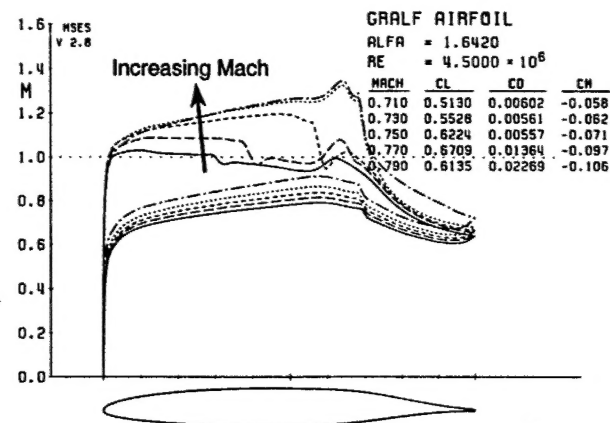


Figure 10: Effect of Mach number at constant α .

4.2 Boundary Layer Stability Analysis

Innovative Aerodynamic Technologies' LAMDA (Laminar Airfoil Manager for Design and Analysis) package¹¹ was used to evaluate the three-dimensional boundary layer stability characteristics of the swept GRALF airfoil. It was also used as a method to check the aerodynamic characteristics and the basic airfoil stability characteristics provided by the MSES code.

LAMDA assembles an airfoil flow analysis code, boundary layer analysis codes, and laminar boundary layer stability analysis and transition prediction codes under a user-friendly graphical user interface (GUI). The tool is designed to allow an inexperienced user to conduct a reliable two-dimensional incompressible stability analysis, and can reduce a typical analysis effort from days to hours. Tollmien-Schlichting (T-S) and crossflow (CF) instabilities are considered. A graphics package is included, which allows the user to quickly plot and examine relevant data. A description LAMDA is given here due to the lack of published material on the code.

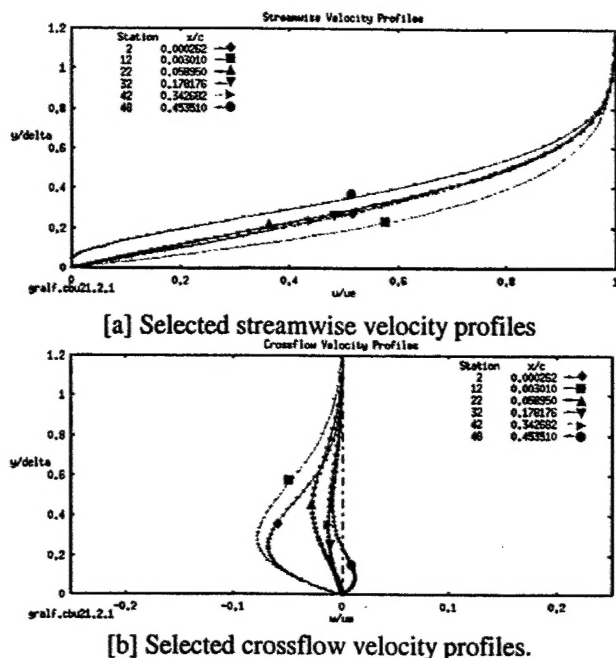


Figure 11: Selected upper surface boundary layer profiles upstream of the shock at design conditions ($C_L=0.62$, $Re=4.5 \times 10^6$, $\Lambda_{LE}=20^\circ$).

4.2.1 Mean Flow Prediction Method

The flow analysis method currently included in the LAMDA tool is the "NYU" code developed by Bauer, Korn, & Garabedian^{12,13,14}. This 2-D transonic analysis code solves the full potential equations in non-conservative form using rotated finite difference shock scheme. The code assumes the two-dimensional, steady, isentropic irrotational flow of inviscid, polytropic gas. The resulting equations of motion are transformed into the complex plane and then solved numerically.

The program uses the user-specified airfoil coordinates along with a specified freestream Mach number, lift coefficient (or angle of attack), and the leading and trailing edge sweep angles. It then provides an inviscid pressure distribution about the airfoil for these conditions. The method may also be used in a pseudo-viscous mode by including the boundary layer displacement thickness. If the boundary layer is to be included, the user must provide the Reynolds number and the transition locations on the upper & lower surfaces. The NYU Airfoil Flow Solver is a robust potential flow solver with simple inputs. It is fast to run and has been successfully used as an input solver to the boundary layer analysis code in the past.

LAMDA also has the "hooks" to use MSES or MSIS as the flow prediction tool. This version was, however, not available to us at the time of this analysis. It would have the primary advantage of being coupled with a transition prediction capability in a closed-loop manner.

4.2.2 Boundary Layer Analysis Method

The Kaups & Cebeci boundary layer code¹⁵ was used to compute the boundary layer profiles on the airfoil. It is a compressible code with conical assumption 3-D capability. However, in the version 1.0 LAMDA package only the 2D incompressible analysis is conducted. The code, which generates the laminar boundary layer velocity profiles, is used as the standard input to the stability analysis code, SALLY. The full potential of the Kaups & Cebeci code to handle tapered wings is not exploited in LAMDA at this date. The BLSTA code of Yong-Sun Wie¹⁶ is also provided as optional boundary layer solvers. Streamwise and crossflow velocity profiles through the boundary layer as predicted by LAMDA (i.e. the Kaups & Cebeci boundary layer code) for the GRALF at design conditions are shown in Figure 11

4.2.3 Stability & Transition Prediction Method

At the heart of LAMDA are the boundary layer stability analysis tools. Methods currently available through LAMDA are the widely known SALLY, COSAL¹⁷, and MARIA codes. For the present study, only the COSAL results are discussed. COSAL is a three-dimensional compressible temporal stability code used for transition prediction over airfoils and wings. It computes the compressible linear stability characteristics and integrates the amplification rates of the boundary layer disturbances.

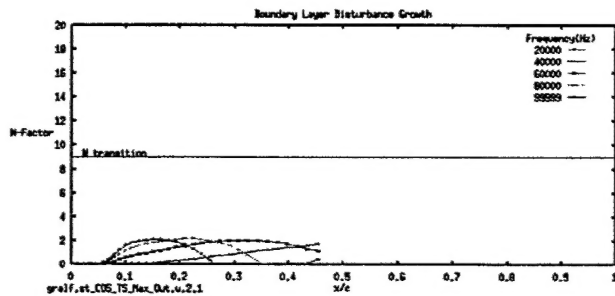
The linear stability analysis of compressible boundary layers involves solution of an eigenvalue problem for an eighth-order system of differential equations. The basic equations for the linear stability analysis are derived using small disturbance theory. If the mean flow is assumed to be locally parallel, one obtains a set of five ordinary differential equations (three second-order momentum equations, a second-order energy equation, and a first-order continuity equation). COSAL employs a finite-difference method to solve the compressible stability equations in their original form. COSAL includes two eigenvalue search procedures. A global procedure is provided for use when no initial guess is available, and a fast local eigenvalue search procedure is used when an initial estimate is provided by the user or global search.

COSAL calculates the local disturbance growth rate, and uses the " e^N " method¹⁸ obtained by integrating the local disturbance growth. The local growth rate obtained is temporal and must be converted to a local spatial growth rate by using local group velocity before it can be integrated. The N -factor (the logarithmic amplification ratio of linear disturbances within the boundary layer) is used for transition correlation for swept and tapered laminar flow wings. The N -factor method predicts transition based on the growth of disturbances. The local growth rate can be obtained by using different approaches. Two of the following parameters must be fixed: disturbance frequency, wavelength, orientation angle, or span-wise wavenumber. Or, as was used in the

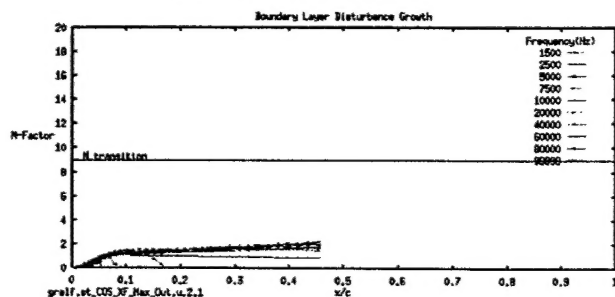
present study, the disturbance frequency can be fixed while the growth rate is maximized. For swept wing calculations using COSAL, it is typical for the maximum growth rate to be CF in the initial acceleration region, then switch to T-S as the pressure distribution flattens out. In the present analysis, a new LAMDA option was used which forces the tracking to follow a fixed type of disturbance. Hence, the code does not allow the type of disturbance that is being tracked (T-S or CF) to change.

The LAMDA tool actually uses Innovative Aerodynamic Technologies' own version of the COSAL code (called COSAL-IAT). In this version, several improvements have been made to make it more robust, and to minimize the user inputs required to obtain a valid solution. Information is also provided early in the analysis that helps the user choose appropriate starting values and parameters for the stability analysis. The COSAL code has also been made more robust when calculating through the damping region. Previously, the code often lost track of a disturbance and had problems quantifying its damping in stable regions. The selection of the type of disturbance that will be amplified and tracked (T-S or CF), as well as how it is to be amplified have all been simplified by the GUI.

Input to COSAL consists of boundary layer profile data, control parameters, and stability problem description parameters. Output from COSAL includes displacement thickness, non-dimensional complex frequency, and disturbance amplitude ratio (local growth rate).



[a] T-S disturbance growth.



[b] CF disturbance growth.

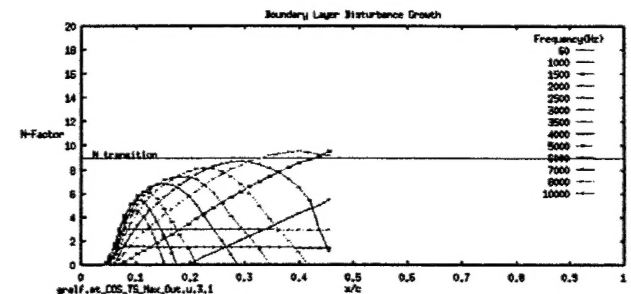
Figure 12: Upper surface disturbance growth for selected frequencies at design conditions ($C_L=0.62$, $Re=4.5 \times 10^6$, $\Lambda_{LE}=20^\circ$).

4.2.4 Boundary Layer Stability Predictions

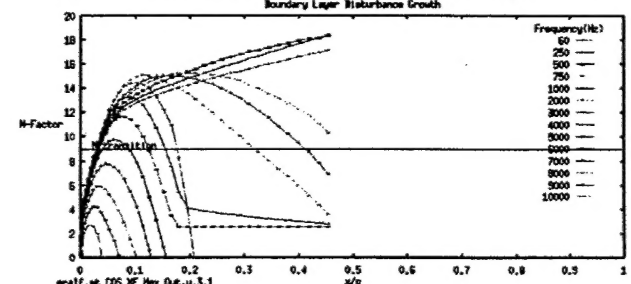
Predicted C-F and T-S disturbance growth curves are presented for the GRALF airfoil at the design condition in Figure 12. The growth of disturbances in both T-S and CF analyses are well within the design criteria. Disturbance "N-factors" are predicted to remain well below 2.5 until the shock is encountered. As will be discussed in Section 5.2, this shock was predicted by LAMDA (the NYU code) to be forward of the MSES prediction, and very close to the measured location. Based on this second stability analysis, no boundary layer stability problems would be expected in the tunnel. Furthermore, sweeping the airfoil 20° on an aircraft should introduce no major crossflow instability issues.

It should be noted that we would have liked to investigate slightly higher frequencies. Since the boundary layer on a wind tunnel model will be very thin, the disturbance wavelengths of interest will be very small, requiring the analysis of very high (dimensional) frequencies. Due to formatting restrictions in the LAMDA GUI, it is very difficult to analyze frequencies above 100kHz.

The boundary layer stability was also investigated at several other Reynolds numbers. The results indicate that the amplification of the T-S instabilities are satisfactory up to a flight Reynolds number of about 30×10^6 . However, at this condition, the CF instability amplifications are unacceptable (Figure 13), causing transition very near the leading edge.



[a] T-S disturbance growth for selected frequencies.



[b] CF disturbance growth for selected frequencies.

Figure 13: Upper surface stability analysis results from LAMDA at high Reynolds number ($C_L=0.62$, $Re=30 \times 10^6$, $\Lambda_{LE}=20^\circ$).

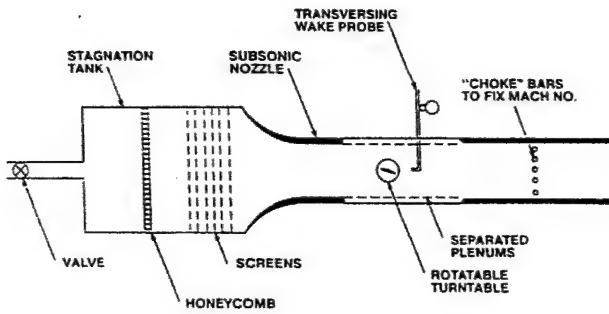


Figure 14: Schematic of OSU Low Turbulence Wind Tunnel Facility.

5 Wind Tunnel Experimental Validation

Highly instrumented high Reynolds number airfoil wind tunnel tests were performed at the Ohio State University (OSU) Aeronautical and Astronautical Research Laboratory (AARL) to validate the GRALF airfoil design. The airfoil was evaluated at a Reynolds number of 4.5 million and included Mach numbers from 0.4 to 0.77. The range of angle-of-attack was from -2° to 6° . Surface pressures and traversing wake probe data were collected for each of the models and from these data, lift, drag and pitching moment coefficients were calculated.

5.1 Experimental Technique

5.1.1 Facility

Experimental validation of this airfoil design was performed in The Ohio State University 6x22 inch blow-down transonic wind tunnel. This facility has a proven track record in the developmental airfoil validation testing area, including several NLF airfoil experiments, and is among the lowest turbulence level transonic wind tunnels in US. It is capable of sustaining Mach numbers from 0.2 to 1.1 and chord Reynolds numbers from 2-12.5 million. The facility uses a complete instrumentation suite for obtaining accurate lift, moment, and drag measurement. Access flanges are on both sides for easy installation, inspection, and cleaning. A complete description of the test facility and its characteristics can be found in Reference 19.

5.1.2 Airfoil Models

The two models were used to test GRALF airfoil design. One model was instrumented with surface pressure taps (several small pressure ports on the airfoil surface) at 52 locations (shown in Figure 15). Since pressure taps tend to prematurely trip the boundary layer, a second model with no pressure taps was used to measure "natural transition" drag. Both models had a 6-inch span and a 6-inch chord length. The tapped model was also tested in a second "tripped" configuration, where the boundary layer was forced to transition early.

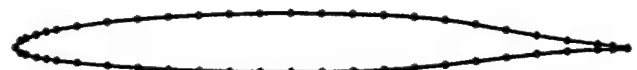


Figure 15: Distribution of pressure taps on GRALF model.

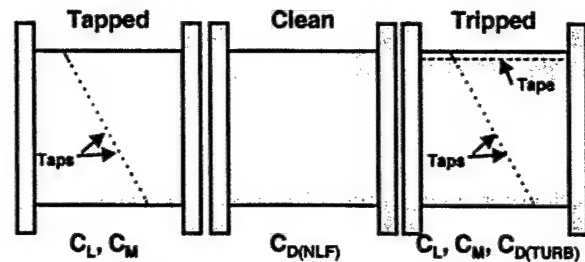


Figure 16: Wind tunnel model configurations tested.



Figure 17: Airfoil model in test section.

5.1.3 Data Acquisition & Reduction

Surface pressure measurements and wake survey data were acquired for these tests. A complete description of the scanivalve data acquisition system can be found in Reference 19. From the surface tap measurements, the lift, pressure drag and pitching moment were calculated by integrating surface pressures over the airfoil. Total drag is calculated from the wake survey pressure measurements. The momentum deficit is integrated across the wake to compute the total drag.

To obtain drag estimates for natural transition, the "clean" model (with no pressure taps) was used. During these experiments, the model was carefully cleaned at regular intervals, and inspected for condensation and other surface irregularities. The natural transition experiments were reserved for days with dry weather conditions.

5.2 Results

Several plots of the lift, drag, and pitching moment coefficients for the GRALF follow. Selected surface pressure distributions are also used to illustrate airfoil characteristics. While only selected cases are shown here, a fairly extensive set of tunnel data has been collected.

5.2.1 Comparisons of Predictions & Measurements

Shown in Figure 18 are the measured performance data for the GRALF airfoil at its design condition. Also shown are corresponding MSES predictions. The most noticeable discrepancy is the slope of the lift curve. While the predicted and measured zero-lift angle of attack (α_0) agree quite well, the predicted slope ($C_{L\alpha}$) is discernibly higher (0.20) than the measured value (0.16). This has difference been seen in previous tests conducted at the OSU facility, and tends to increase with higher Mach numbers. Sidewall corrections to effective airfoil incidence may need to be investigated. Despite this, when comparisons are based on equivalent C_L (as will be done henceforth), measurements compare well to predictions. For example, MSES proved to be quite accurate in the prediction of drag as a function of lift.

The free-transition drag measurements (taken on the clean model) are denoted "Natural" in the Figure 18. The measured data compare quite well with MSES predictions over a large range in lift. A few experimental data points actually "fell into" the predicted laminar drag bucket near $C_L=0.2$. Near the design point ($C_L=0.62$) we were unable to measure quite as low of drag values as were predicted. This leads directly to the over-prediction of lift-to-drag ratio (Figure 19), and ultimately range.

This may be due to the differences between the shock location predicted by MSES and those observed in the tunnel near the design lift condition (Figure 20). At the design point, the shock location measured in the tunnel (symbols) was further forward than predicted (dark lines).

Table 5: Predicted and measured aerodynamic properties for the GRALF airfoil near the design C_L .

Parameter	Predicted (MSES)	Measured
Mach number	0.75	0.751
Reynolds number	4.5×10^6	4.459×10^6
C_L	0.620	0.613
C_M	-0.07058	-0.0631
C_D	0.00562	0.0070
α	1.64	2.8
L/D	110.1	91.8

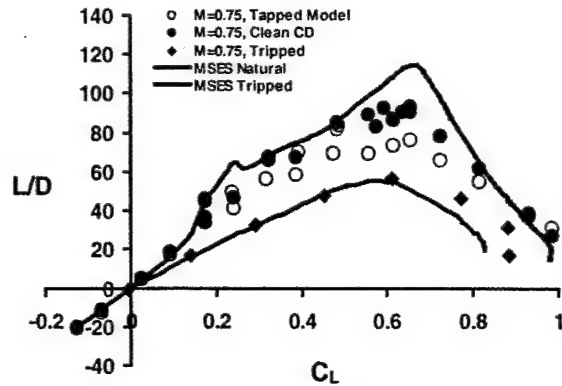


Figure 19: Predicted and measured L/D ratios.

As discussed in Section 4.1, this would force transition location on the upper surface forward, leading to slightly higher friction drag. However, the pressures of the shock compare quite well, and the shock strengths are comparable, leading to a reasonable drag prediction.

This issue has been experienced before²⁰ in the facility, and it has been suggested that additional Mach number corrections may need to be addressed in the data reduction that could influence the high-lift high-Mach cases. (The extreme sensitivity of the shock location to

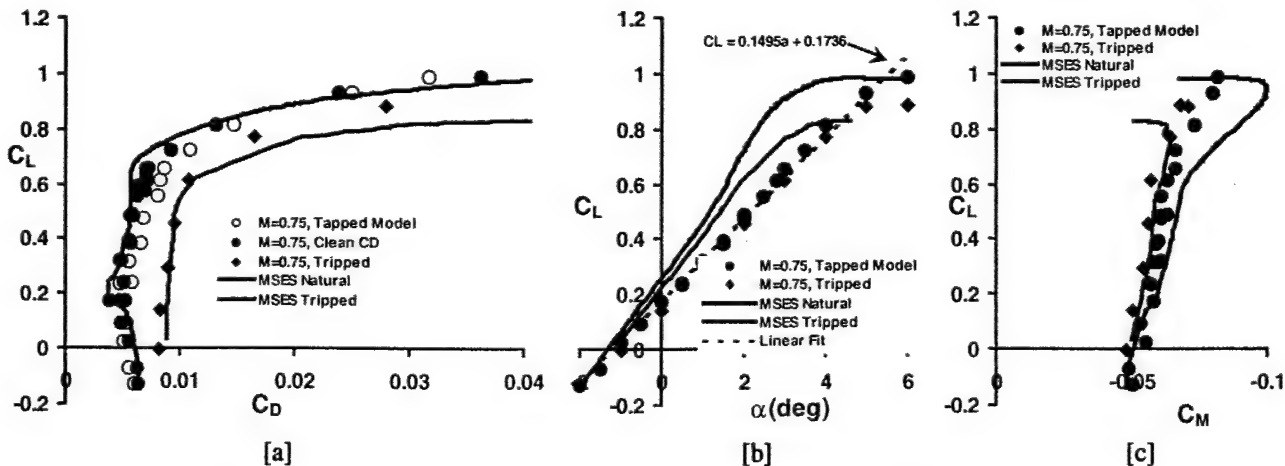


Figure 18: Predicted and measured airfoil performance at $M=0.75$, $Re_c=4.5 \times 10^6$. Experiments were conducted at $M=0.751 \pm 0.002$, $Re_c=(4.50 \pm 0.05) \times 10^6$.

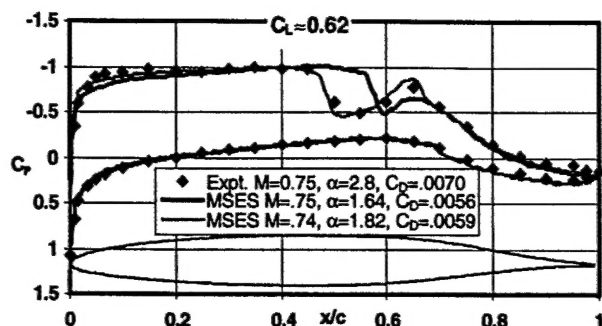


Figure 20: Predicted and measured surface pressure distribution at design C_L (0.62).

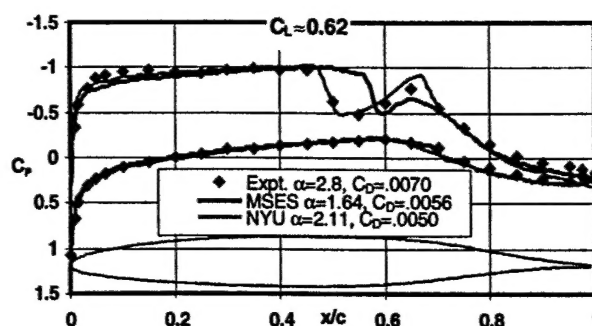


Figure 22: Predicted and measured pressure distribution at design C_L (0.62) and Mach number (0.75).

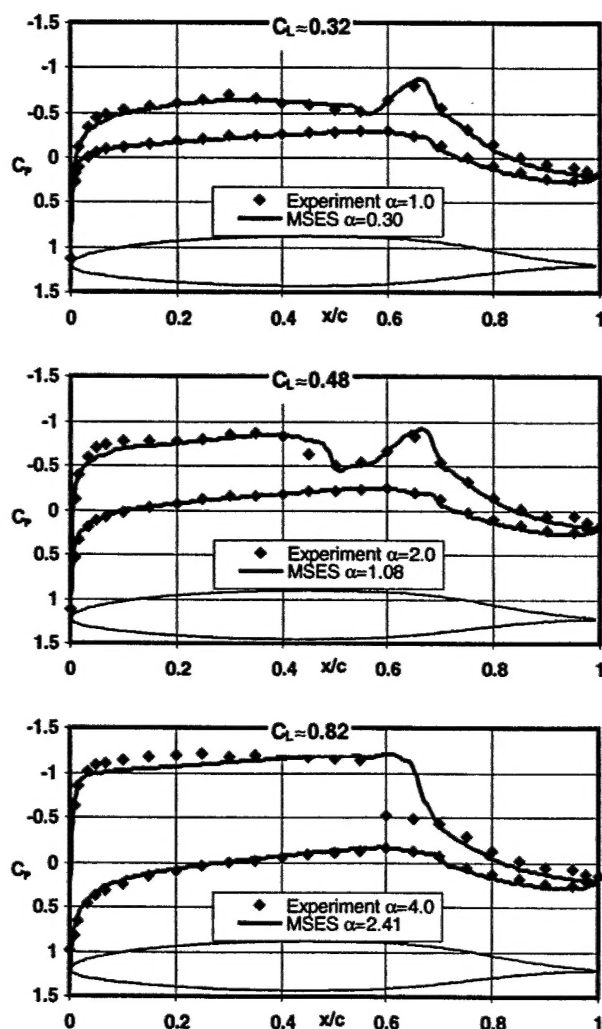


Figure 21: Predicted and measured surface pressures at off-design lift conditions.

freestream Mach number near the design condition was illustrated in Figure 10.) To demonstrate, an MSES solution was obtained at the same lift coefficient, but a slightly lower Mach number of 0.74. The resulting

pressure distribution (light line in Figure 20) is nearly identical to the measured pressures. The predicted incidence required to produce the design lift coefficient, and the predicted drag coefficient, are also closed to the measured values. At lower lift conditions, the measured and predicted shock locations compare much more favorably (Figure 21), as do the drag values (Figure 18).

While this is compelling evidence that a Mach correction should be looked into, there is some evidence to the contrary. At the design condition, the NYU code (within LAMDA) gave surface pressure predictions that were more consistent with the experiment. For the solution shown in Figure 22, the boundary layer was forced to transition at the locations predicted by MSES. Nearly the same pressure distribution is predicted if the NYU code and COSAL are "hand-iterated" to find its own transition locations (a very tedious process), or the NYU module is simply run in an inviscid mode. However, the NYU code actually predicted less drag at this condition than MSES, further away from the measured value. The differences between MSES and NYU solutions are still being investigated. Discrepancies are probably related to differences in the external flow solver, external grid-generation methods, or are user related.

The drag measurements at $0 \leq C_L \leq 0.2$ indicated that an assumed N_{crit} of 5-7 might have been more suitable for the lower surface (see Figure 7). The assumed N_{crit} of 4 appears to have been a wise choice for the upper surface.

Although the drag measurements on the tapped model are of little interest for NLF airfoils, these measurements also shown (open symbols) to show the influence of the pressure taps on the boundary layer stability, and hence the measured drag.

The measured zero-lift pitching moment (C_{M0}) agree very well with the predictions made with MSES. Considering the magnitude of the moment, the slope was also predicted quite well. No severe breaks in the moment data are seen in the experimental data at high lift, indicating there is no boundary layer separation. This is desirable for controllability at high-lift conditions.

5.2.2 Off-Design Investigations

During operations, laminar flow airfoil will occasionally encounter insects and clouds (ice crystals)²¹. They sometimes operate in noisy conditions created by the aircraft. Aircraft are often forced to fly at off-design Reynolds number and Mach number to suit mission requirements. For these reasons, it is critical to assess the airfoil performance at off-design conditions. For these reasons, the robustness of the airfoil performance to off-design conditions was investigated.

Premature transition (due to insects, dirt, icing, cloud encounters, aging surfaces, noise, etc.) was simulated experimentally by wrapping a piece of 5/8-inch wide "Magic tape" to the leading edge of the airfoil. This created a backward-facing step at $0.05c$ on the upper and lower surfaces that produced a turbulent boundary layer. The method has been used on many previous tests as a minimum-disturbance trip device. This condition is easily simulated in MSES by specifying a corresponding transition location. While the free-transition drag measurements are of the most interest for NLF airfoils, the "tripped" results shown Figure 18 show that MSES does a very good job of predicting turbulent airfoil drag as well. In terms of cruise performance, it can be seen that the airfoil performs much more poorly with the tripped boundary layer (Figure 18 & Figure 19).

A common concern in the design of NLF airfoils is the effect that a sudden transition to fully turbulent flow can have on the stability and trim characteristics, as transition is often accompanied by a large change in moment coefficient. For this airfoil, tripping the boundary layer at $5\%c$ was predicted to have relatively mild effects by both all methods employed (see Figure 18).

Reynolds number effects have been investigated numerically with MSES. The effect of increasing the Reynolds number (larger chord or lower altitude) on the airfoil's performance is illustrated in Figure 23. Here, an N_{crit} of 9 was chosen. Maximum L/D is actually improves with increasing Reynolds number over most of the range investigated. In practice, the airfoil would be redesigned for the higher Reynolds number flight condition of the global range transport. Note that the predicted transition location of $x/c=0.3$ is very close to where the disturbance

growth envelope predicted for the T-S stability boundary with LAMDA reaches an N -factor of 9 (see Figure 13[a]).

The robustness of the airfoil to perform at off-design Mach numbers was also tested analytically and experimentally. The effects of Mach number (as well as tripping the boundary layer) are summarized in Figure 24–Figure 26. Figure 24 and Figure 25 represent the aircraft flying at slightly off-design Mach numbers to meet time constraints or other mission requirements. Lowering Mach number to 0.71 introduces no problems, and improves the agreement between tunnel data and MSES predictions. Increasing the Mach number to 0.77 has the primary unwanted effects of increasing the C_{Ma} slope, creating moment problems at high C_L . It also intensifies the undesirable effects of tripping the boundary layer.

The case in Figure 26 represents a lower-speed loiter or approach condition. Performance is still acceptable, but the maximum C_L is very limited, and the stall is predicted to be quite abrupt. We are currently looking into flapped versions of the GRALF airfoil using MSES's multi-element capability. Active flow control is a likely technology to enhance (or recover) performance at off design conditions. This is especially true of separation control to improve high-lift performance.

In all, the results show that the GRALF airfoil is a promising design. Both MSES and wind tunnel results indicate very good off-design performance. The airfoil exhibits a low zero-lift moment coefficient and safe behavior at off-design points and in "turbulent mode".

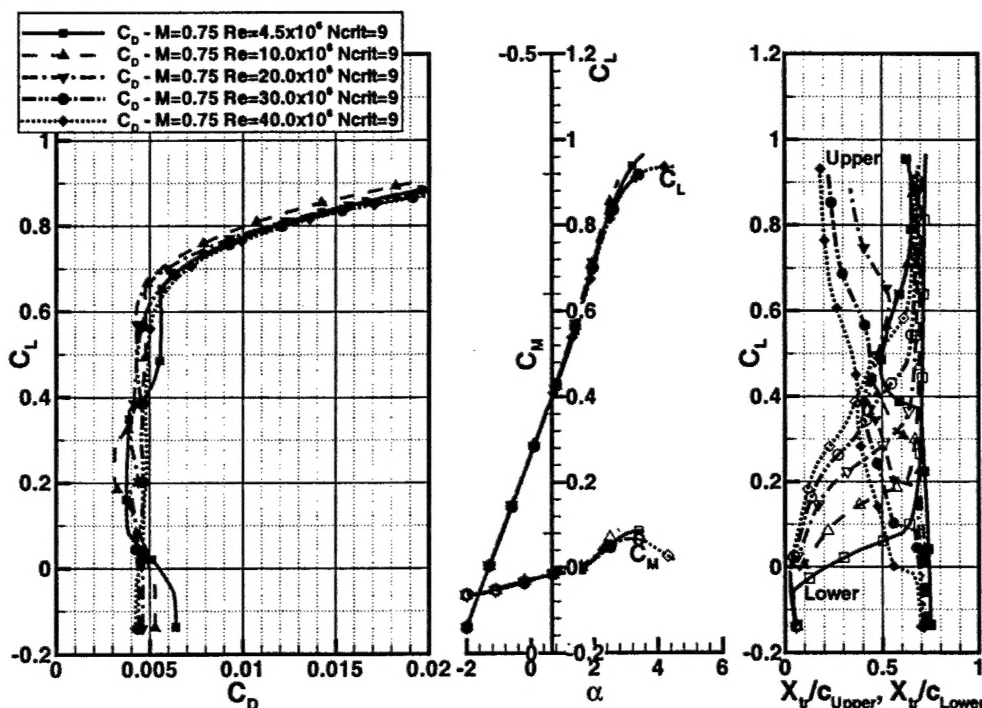


Figure 23: Effect of Reynolds Number on airfoil performance predictions from MSES.

6 Continuing Efforts

A database of airfoils currently used on military transport aircraft has also been developed using the MSES code. This information is now being used as a baseline to judge performance improvements offered by new airfoil designs against, starting with the GRALF airfoil. Results at typical points of the flight envelope for existing and original airfoils have been compared²².

Once the airfoil boundary layer stability characteristics are understood, it is possible to evaluate the airfoil using conventional finite-difference or finite-volume CFD methods. Reynolds-Averaged Navier Stokes (RANS) solutions are being obtained for several operating conditions. Several orders of differencing, inviscid flux models, and levels of turbulence modeling are being

investigated using the commercial GASP²³ code. The inviscid solutions obtained to date provide reasonable lift and moment estimates. However, the predicted pressure drag, as would be expected, is lower than was measured. The viscous RANS simulations are still underway, and it is premature to evaluate the results. So far, MSES has provided superior drag predictions to any other method, while predicting the moment as well.

Much of our future airfoil development at AFRL will focus on high-altitude (low Reynolds number) UAV applications. The challenge will be to maximize on-station time (loiter) while meeting the geometric constraints imposed by the sensor package. These aircraft may also operate at high Mach numbers; similar to the transport described in this paper.

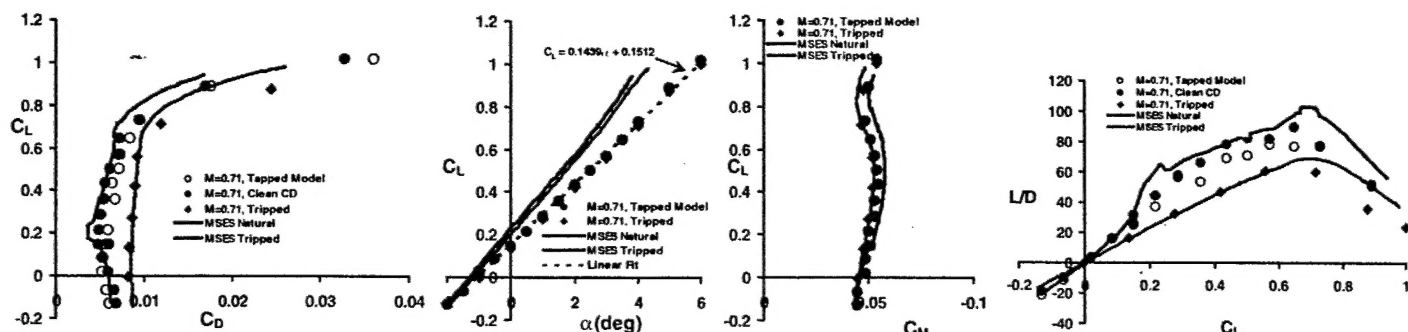


Figure 24: Predicted and measured airfoil performance at $M=0.71$, $Re_c=4.5 \times 10^6$, $N_{crit}=4$. Experiments were conducted at $M=0.71 \pm 0.002$, $Re_c=(4.50 \pm 0.05) \times 10^6$.

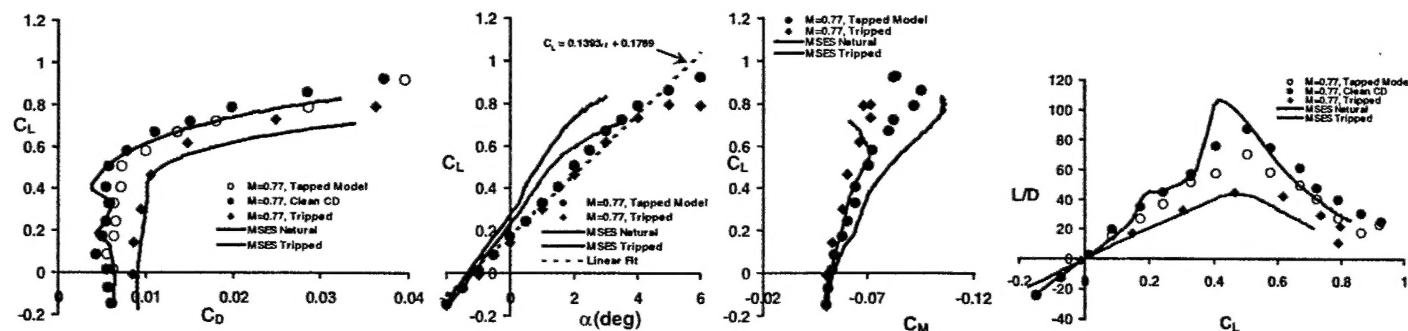


Figure 25: Predicted and measured airfoil performance at $M=0.77$, $Re_c=4.5 \times 10^6$, $N_{crit}=4$. Experiments were conducted at $M=0.770 \pm 0.001$, $Re_c=(4.50 \pm 0.06) \times 10^6$.

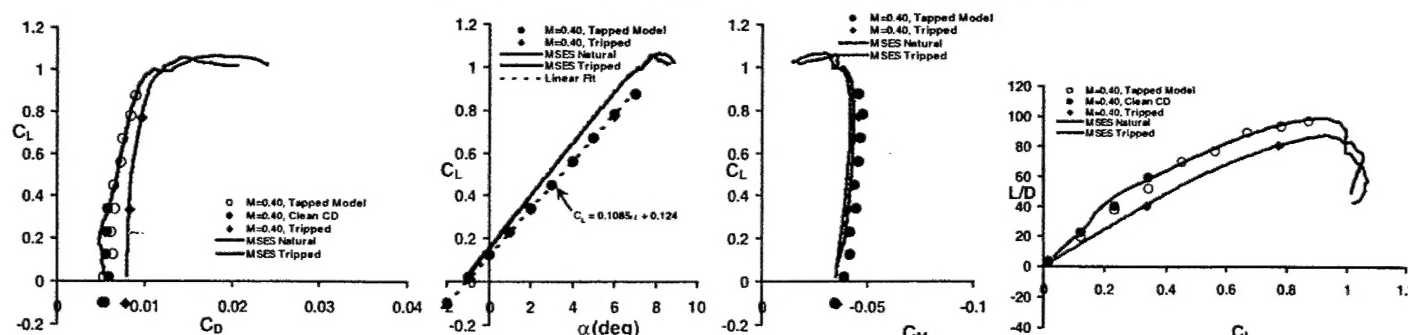


Figure 26: Predicted and measured airfoil performance at $M=0.40$, $Re_c=4.5 \times 10^6$, $N_{crit}=4$. Experiments were conducted at $M=0.770 \pm 0.001$, $Re_c=(4.50 \pm 0.06) \times 10^6$.

7 Summary

The use of laminar flow technology on future aircraft could lead to enhancement of performance, reduction of operational cost, and reduction of environmental impact. We have described, in this paper, the developmental process for an airfoil to be used on long-range transonic transport aircraft having large regions of laminar flow. An airfoil with a natural laminar flow low drag bucket had been designed and validated for a relatively high-speed transonic long-range transport configuration. Drag levels of 56-70 counts or less were measured over a lift coefficient range of 0 to 0.66. The desired negative zero-lift moment coefficients were demonstrated in the wind tunnel, as was the mild increase in moment magnitude with lift. The indifference of moment to tripping the boundary layer was also demonstrated, thereby ensuring no adverse effects on controllability during adverse conditions. In fact, the airfoil has no indication of separation near cruise lift coefficients under fully turbulent conditions. The robustness of the airfoil to perform at off-design Mach numbers with no significant performance penalties was also verified. Crossflow stability and transition issues have also been addressed using a commercial laminar airfoil design and analysis tool (LAMDA). The MSES code proved to be an effective tool for NLF airfoil design and analysis when used wisely. In particular, the ability to predict drag and moment over a wide range of lift has been demonstrated.

8 Reference

- ¹ *New World Vistas — Air and Space Power for the 21st Century*, USAF Scientific Advisory Board, 1995.
- ² Tilmann, C. P. & Osborn, R. F., "Active Flow Control for Drag Reduction at AFRL's Aerodynamic Configuration Branch," *Proceedings of the 17th Canadian Congress of Applied Mechanics*, Hamilton, Ontario, June 1999.
- ³ Tilmann, C. P. & Osborn, R. F., "Active Control of Separation at AFRL's Aerodynamic Configuration Branch," *Proceedings of the 17th Canadian Congress of Applied Mechanics*, Hamilton, Ontario, June 1999.
- ⁴ Selig, M. S., and Maughmer, M. D., "A Multi-Point Inverse Airfoil Design Method Based on Conformal Mapping," *AIAA Journal*, Vol. 30, No. 5, pp.1162-1170, May 1992.
- ⁵ Drela, M., "Design and Optimization Method for Multi-element Airfoils," *AIAA-93-0960*, January 1993.
- ⁶ Herling, W. W., LeDoux, S. T., Ratcliff, R. R., Treiber, D. A., Warfield, M. J., Emsley, H. T. "3DOPT — An integrated system for aerodynamic design optimization," *AIAA-98-2514*, June, 1998
- ⁷ Logan, M. J., "2020 — Future vision for Global Air Cargo," *AIAA-98-0437*, Jan. 1998.
- ⁸ Drela, M., "Two-Dimensional Transonic Aerodynamic Design and Analysis Using the Euler Equations," Ph.D. Dissertation, MIT GTL Rept. No. 187, Feb. 1986.
- ⁹ Drela, M., Giles, M. B., "ISES: A Two-Dimensional Viscous Aerodynamic Design and Analysis Code," *AIAA-87-0424*.
- ¹⁰ Drela, M., "A User's Guide to MSES 2.8," May 1995.
- ¹¹ LAMDA Laminar Airfoil Manager : Design & Analysis reference "A User-Friendly Graphical User Interface Package for Laminar Airfoil Design," <http://agate.larc.nasa.gov/SBIR/sbr15695.html>, 1998.
- ¹² Bauer, F., Garabedian, P., & Korn, D., "A theory of Supercritical Wing Sections, with Computer Program and Examples," New York, Springer-Verlag, 1972
- ¹³ Bauer, F., Garabedian, P. R., Korn, D., & Jameson, A. "Supercritical Wing Sections II," in *Lecture Notes in Economics and Mathematical Systems : 108*, Springer-Verlag, New York, 1975.
- ¹⁴ Bauer, F., Garabedian, P., & Korn, D., "Supercritical wing sections III," in *Lecture notes in economics and mathematical systems : 150*, Springer-Verlag, New York, 1977.
- ¹⁵ Kaups, K., & Cebeci, T., "Compressible Laminar Boundary Layers with Suction on Swept and Tapered Wings," *Journal of Aircraft*, Vol. 14, pp. 661-667, July 1977.
- ¹⁶ Wie, Yong-Sun, "BLSTA — A Boundary Layer Code for Transitional Analysis," NASA CR-4481, 1991.
- ¹⁷ Malik, M. R., "COSAL — A Black Box Compressible Stability Analysis Code for Transition Prediction in Three Dimensional Boundary Layers," NASA CR-165925, May 1982.
- ¹⁸ Smith, A. M. O., "On the Growth of Taylor-Görtler Vortices Along Highly Curved Walls," *Quarterly Applied Mathematics*, Vol XIII, pp.233-262, Oct. 1955.
- ¹⁹ Lee, J. D., Gergorek, G. M., & Korkan, K. D., "Testing Techniques and Interference Evaluation in the OSU Transonic Airfoil Facility," *AIAA-78-1118*, July 1978.
- ²⁰ Brandt, L., & Stone, T., "2-D Airfoil Tests," Lockheed Aeronautical Systems Company Report No. SP-6863, January 1990.
- ²¹ Wagner, R. D., Maddalon, D. V., & Fisher, D. F., "Laminar Flow Control Leading Edge Systems in Simulated Airline Service," *ICAS 88-3.7.4*, September 1988.
- ²² Höhn, T., & Tilmann, C. P., "Inviscid/Viscous Analysis of Transonic Airfoils for Long Range Transport Aircraft," 24th AIAA Symposium on Aerospace Science and Technology, Dayton, OH, April 1999.
- ²³ "The General Aerodynamic Simulation Program, Version 3 Users Manual," Aerosoft Inc. (www.aerosoft.com), Blacksburg, Virginia. 1996.